

The Johnson-Segalman model with a diffusion term in cylindrical Couette flow*

P. D. Olmsted, O. Radulescu^{1†} and C.-Y. D. Lu²

¹Department of Physics and Astronomy, and IRC in Polymer Science and Technology, University of Leeds, Leeds LS2 9JT, United Kingdom;

²Department of Physics, National Central University, Chung-li, Taiwan 320, Republic of China

We study the Johnson-Segalman (JS) model as a paradigm for some complex fluids which are observed to phase separate, or “shear-band” in flow. We analyze the behavior of this model in cylindrical Couette flow and demonstrate the history dependence inherent in the local JS model. We add a simple gradient term to the stress dynamics and demonstrate how this term breaks the degeneracy of the local model and prescribes a much smaller (discrete, rather than continuous) set of banded steady state solutions. We investigate some of the effects of the curvature of Couette flow on the observable steady state behavior and kinetics, and discuss some of the implications for metastability.

1. INTRODUCTION

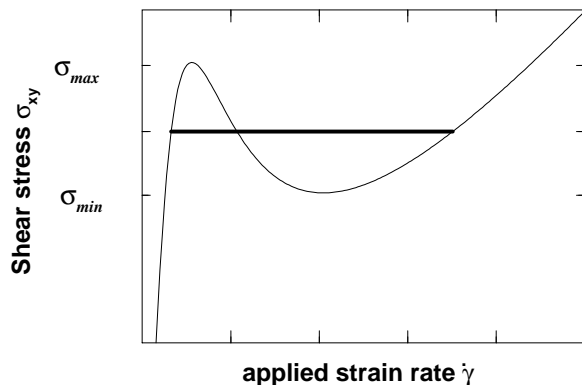


FIG. 1. Local constitutive relation for the JS model (Eq. 3.1). The horizontal line shows a possible stress for banded flow, with material on either the low or high strain rate branches. The negative slope portion of the curve represents mechanically unstable homogeneous flows.

Non-analytic flow behavior is seen in a wide range of complex fluids, including polymer melts (Bagley, Cabot and West, 1958; Vinogradov, 1972), wormlike micelles (Berret, Roux and Porte, 1994; Callaghan, Cates, Rofe and Smeulders, 1996; Grand, Arrault and Cates, 1997; Boltenhagen, Hu, Matthys and Pine, 1997), and lamellar surfactant phases (Roux, Nallet and Diat, 1993; Diat, Roux and Nallet, 1993; Diat, Roux and Nallet, 1995; Sierro and Roux, 1997). In the “spurt effect” in pipe flow (Bagley et al., 1958; Vinogradov, 1972) the flow rate increases discontinuously above a given applied pressure gradient. In Couette flow this behavior manifests itself in non-analyticities in the steady state flow curves of wall stress as a function of relative cylinder veloc-

ity, with either a discontinuity or a discontinuous first derivative in the apparent constitutive curve. In some worm-like micellar solutions this flow behavior coincides with a range of strain rates for which macroscopic phase separation is observed (Berret et al., 1994; Callaghan et al., 1996; Grand et al., 1997) under controlled strain rate conditions, with stresses on a well defined, reproducible, and history-independent plateau.

Although wall slip or internal fracture, rather than bulk instability, has been suggested to explain the spurt effect (Denn, 1990), bulk phase separation is undisputed in the wormlike micelle system. This phenomenon has often been interpreted in terms of a non-monotonic constitutive curve analogous to a van der Waals loop, as in Fig. 1. Here σ_{xy} is the shear component of the fluid stress tensor, x is the coordinate in the flow direction, and y is in the gradient direction. There are many kinds of non-monotonic behavior (Porte, Berret and Harden, 1997; Olmsted and Lu, 1997), and we focus here on systems with multiple strain rates for a given stress. Constitutive curves of this character are found in the phenomenological Johnson-Segalman (JS) model (Johnson and Segalman, 1977; Malkus, Nohel and Plohr, 1990; Malkus, Nohel and Plohr, 1991), the Doi-Edwards microscopic reptation model for polymers (Doi and Edwards, 1989) and the similar model of Cates (1990) for wormlike micelles (both augmented with a stabilizing high shear-rate branch), and other recent models for branched polymers (McLeish and Larson, 1998). These flow curves have regions of negative slope, $d\sigma_{xy}/d\dot{\gamma} < 0$, which are hydrodynamically unstable. For applied strain rates in these unstable regions, a reasonable scenario consistent with experiments is for the system to break up into bands of different flow rates, each band lying on a stable part ($d\sigma_{xy}/d\dot{\gamma} > 0$) of the curve. This possibility has been studied for various models of non-Newtonian fluids

*To be published in *Journal of Rheology*

[†]p.d.olmsted@leeds.ac.uk, phyor@irc.leeds.ac.uk, dlu@joule.phy.ncu.edu.tw

(McLeish and Ball, 1986; McLeish, 1987; Olmsted and Goldbart, 1992; Spenley, Yuan and Cates, 1996; Olmsted and Lu, 1997). However, the stress can apparently lie anywhere within a range of stresses. This degeneracy of *selected* stresses has engendered much discussion, and is at odds with the wormlike micelles, which shear-band at a well-defined stress that is independent of flow history (Berret et al., 1994; Callaghan et al., 1996; Grand et al., 1997; Boltenhagen et al., 1997).

Most experiments are performed under conditions which impose inhomogeneous stress. For example, in pressure-driven (Poiseuille) pipe flow the steady state shear stress varies linearly with distance from the center of the pipe, while in cylindrical Couette flow the stress varies as the inverse of the square of the radius. There is a growing body of theoretical work addressing shear banding in inhomogeneous flow conditions; in particular, we are interested in the relationship between the degeneracy of models such as the local JS model, and the possible history-dependence in different flow geometries, and how to resolve this degeneracy.

McLeish (1987) studied the stability and hysteresis of shear banding in a modified local Doi-Edwards fluid in pipe flow, and found that normal stress effects should affect the stability of banded flows. Malkus et al. (1990) and Malkus et al. (1991) studied the local JS model in planar Poiseuille flow and presented a comprehensive phase-plane analysis of the steady state behavior, showing how a hysteresis loop resulted from a particular flow history. Greco and Ball (1997) studied shear banding in start-up flows of the JS model in Couette flow, and demonstrated that the curved geometry of Couette flow produces a simple well-controlled banded flow, in contrast to planar flow, in which start-up calculations of similar local models give an uncontrolled number of bands. More recently the degeneracy of the JS model was studied in cylindrical Couette (Georgiou and Vlassopoulos, 1998) and Poiseuille (Fyrillas, Georgiou and Vlassopoulos, 1999) geometries, with the conclusion in each case that selection of a given banded steady state depends on the initial perturbation.

In this paper we first study the consequences of degeneracy for the history dependence of banded solutions to the local JS model in cylindrical Couette flow by imposing several flow histories. We find, similar to Malkus et al. (1991) and Fyrillas et al. (1999) with the JS model in pipe flow, that the apparent flow curves (in this case, wall stress as a function of relative cylinder, or “gap”, velocity) depend on flow history. We restrict ourselves to four basic flow histories and demonstrate how to produce a continuum of possible solutions. Even in the curved geometry, the solution is unstable with respect to noise in the initial conditions, as in the planar case (Georgiou and Vlassopoulos, 1998). This is in distinct contrast to the many experiments which have found a reproducible and unique selected shear stress in systems as diverse as worm-like micelles and surfactant lamellar phases.

To explore unique stress selection we add an addi-

tional term to the JS model, which could be thought of as stress relaxation by diffusion of differently-strained polymer strands (El-Kareh and Leal, 1989; Goveas and Fredrickson, 1998). Such “gradient terms” are not usually included in constitutive equations, but arise naturally in treatments of hydrodynamics of liquid crystals, binary fluids, and polymer blends, and are expected to be present (albeit small) even in one component melts. Such terms will be most important exactly in the highly inhomogeneous interface between shear bands, and constitute a *singular perturbation* on the equations of motion, with a profound effect on stress selection (Lu, Olmsted and Ball, 1999; Radulescu and Olmsted, 1999). Previous workers have used gradient terms to study stress selection in models for liquid crystals in planar shear flow (Olmsted and Goldbart, 1992; Olmsted and Lu, 1997), and in a one-dimensional scalar model for banded flow in micelle solutions by Spenley et al. (1996). Although we make no claims that the JS model accurately approximates these systems, it is a simple model which possesses the requisite non-monotonic constitutive flow curve and whose dynamics, as suggested by Berret, is compatible to some aspects of kinetics experiments of shear banding in solutions of wormlike micelles (Berret et al., 1994; Berret, 1997).

The outline of this work is as follows. In Section 2 we present the equations for the JS model in Couette flow, including the new diffusion term. In Section 3 we present the results from numerical experiments for prescribed strain rates (gap velocity) and different flow histories in the *absence* of diffusion; and in Section 4 we examine the effect of diffusion, which renders the model more realistic with respect to the body of work on complex fluids which display unique stress selection. We finish with a discussion. In a companion paper (Radulescu and Olmsted, 1999) we analyze the diffusive JS model in Poiseuille and Couette geometries, using asymptotic matching techniques, to analytically support many of the findings in this work.

2. MODEL

2.1. Dynamical Equations

The Johnson-Segalman model has been discussed by many authors (Johnson and Segalman, 1977; Malkus et al., 1990; Malkus et al., 1991; Greco and Ball, 1997). The momentum balance condition for an incompressible fluid is

$$\rho (\partial_t + \mathbf{v} \cdot \nabla) \mathbf{v} = \nabla \cdot \mathbf{T}, \quad (2.1)$$

where ρ is the fluid density, \mathbf{v} the velocity field, and \mathbf{T} the stress tensor. The stress tensor is given by

$$\mathbf{T} = -p\mathbf{I} + 2\eta\mathbf{D} + \boldsymbol{\Sigma}, \quad (2.2)$$

where the pressure p is determined by incompressibility ($\nabla \cdot \mathbf{v} = 0$), η is the “solvent” viscosity, and $\boldsymbol{\Sigma}$ is the

“polymer” stress. We separate the velocity gradient tensor $(\nabla \mathbf{v})_{\alpha\beta} \equiv \partial_\alpha v_\beta$ into symmetric and anti-symmetric parts \mathbf{D} and $\mathbf{\Omega}$, respectively:

$$2\mathbf{D} = \nabla \mathbf{v} + (\nabla \mathbf{v})^T \quad (2.3a)$$

$$2\mathbf{\Omega} = \nabla \mathbf{v} - (\nabla \mathbf{v})^T. \quad (2.3b)$$

The non-Newtonian “polymer” stress is taken to have the form proposed by Johnson and Segalman (1977):

$$\overset{\blacklozenge}{\Sigma} = \mathcal{D}\nabla^2 \Sigma + 2\frac{\mu}{\tau}\mathbf{D} - \frac{1}{\tau}\Sigma, \quad (2.4)$$

where μ is the “polymer” viscosity, τ is a relaxation time, and \mathcal{D} is the diffusion coefficient. The difference from the usual JS model is the added diffusion term. This has been derived due to dumbbell diffusion by El-Kareh and Leal (1989), and is also expected to have non-local contributions due to the spatial extent of macromolecules (Lu et al., 1999). Gradient contributions to the polymer stress of blends due to the latter effect have been derived by Goveas and Fredrickson (1998). The time evolution of Σ is governed by the Gordon-Schowalter time derivative (Gordon and Schowalter, 1972),

$$\overset{\blacklozenge}{\Sigma} = (\partial_t + \mathbf{v} \cdot \nabla) \Sigma - (\mathbf{\Omega} \Sigma - \Sigma \mathbf{\Omega}) - a(\mathbf{D} \Sigma + \Sigma \mathbf{D}). \quad (2.5)$$

The “slip parameter” a was interpreted by Johnson and Segalman as a measure of the non-affinity of the polymer deformation; *i.e.* the fractional stretch of the polymeric material with respect to the stretch of the flow field. For $|a| < 1$ the polymer “slips” and the steady-state flow curve in planar shear is capable of the non-monotonic behavior in Fig. 1.

In this work we consider non-inertial flows (zero Reynolds number limit), for which the momentum balance Eq. (2.1) becomes $\nabla \cdot \mathbf{T} = 0$. Although inertial effects should not affect stationary solutions, they may influence transients at the very early stages of start-up experiments, for which inertia cannot be neglected. Spenley et al. (1996) showed that inertial terms have practically no influence on the later stages of the dynamics, so at timescales of order the characteristic relaxation time τ the transients are correctly described by the non-inertial dynamics. Following Greco and Ball (1997), we assume a flow field with azimuthal symmetry, $\mathbf{v} = v(r, t) \hat{\boldsymbol{\theta}}$ between concentric cylinders of radii $R_1 < R_2$, in cylindrical coordinates $\{r, \theta, z\}$. Integrating the balance condition yields

$$\eta \dot{\gamma}(r, t) + \Sigma_{r\theta}(r, t) = \frac{\Gamma}{r^2} \quad (2.6)$$

$$\equiv \sigma(r, t), \quad (2.7)$$

where we define the local strain rate by

$$\dot{\gamma}(r, t) \equiv r \frac{\partial}{\partial r} \left(\frac{v}{r} \right), \quad (2.8)$$

the integration constant Γ is the torque per cylinder length, and $\sigma(r, t)$ is the inhomogeneous shear stress inside the Couette cell gap. We consider no-slip boundary conditions on the fluid velocity \mathbf{v} , a fixed outer cylinder, and an inner cylinder moving at a prescribed gap velocity V . This implies a global constraint

$$\frac{V}{R_1} = \int_{R_2}^{R_1} \dot{\gamma}(r, t) \frac{dr}{r} \quad (2.9)$$

that may be used to find the torque,

$$\Gamma \frac{R_1^2 - R_2^2}{R_1^2 R_2^2} = 2 \left(\frac{\eta V}{R_1} - \int_{R_1}^{R_2} \Sigma_{r\theta} \frac{dr}{r} \right). \quad (2.10)$$

2.2. Rescaled equations

In cylindrical coordinates the dynamical equations for Σ , Eq. (2.4), become

$$\mathcal{L} \Sigma_{rr} = -(1-a) \dot{\gamma} \Sigma_{r\theta} + \frac{2\mathcal{D}}{r^2} (\Sigma_{\theta\theta} - \Sigma_{rr}) \quad (2.11a)$$

$$\mathcal{L} \Sigma_{\theta\theta} = (1+a) \dot{\gamma} \Sigma_{r\theta} - \frac{2\mathcal{D}}{r^2} (\Sigma_{\theta\theta} - \Sigma_{rr}) \quad (2.11b)$$

$$\mathcal{L} \Sigma_{r\theta} = \frac{\mu}{\tau} \dot{\gamma} - \frac{4\mathcal{D}}{r^2} \Sigma_{r\theta} - \dot{\gamma} \left[\frac{1-a}{2} \Sigma_{\theta\theta} - \frac{1+a}{2} \Sigma_{rr} \right] \quad (2.11c)$$

where

$$\mathcal{L} \equiv \partial_t + \tau^{-1} - \mathcal{D} \nabla^2. \quad (2.12)$$

Next we change variables. We introduce the space variable $x \in (0, 1)$ used by Greco and Ball (1997),

$$r = R_1 e^{qx} \quad (2.13a)$$

$$q = \ln \frac{R_2}{R_1}, \quad (2.13b)$$

and define

$$Z = \frac{1-a}{2} \Sigma_{\theta\theta} + \frac{1+a}{2} \Sigma_{rr} \quad (2.14a)$$

$$W = \frac{1-a}{2} \Sigma_{\theta\theta} - \frac{1+a}{2} \Sigma_{rr} \quad (2.14b)$$

$$S = \Sigma_{r\theta}. \quad (2.14c)$$

We now introduce the following dimensionless variables, where \hat{X} is the dimensionless version of X :

$$\hat{V} = V \frac{\tau}{q R_1} \sqrt{1-a^2} \quad \hat{W} = W \frac{\tau}{\mu} \quad (2.15a)$$

$$\hat{Z} = Z \frac{\tau}{\mu} \quad \hat{\gamma} = \dot{\gamma} \tau \sqrt{1-a^2} \quad (2.15b)$$

$$\hat{S} = S \frac{\tau}{\mu} \sqrt{1-a^2} \quad \hat{\mathcal{D}} = \mathcal{D} \frac{\tau}{q^2 R_1^2} \quad (2.15c)$$

$$\hat{\Gamma} = \Gamma \frac{\tau}{\mu R_1^2} \sqrt{1-a^2}. \quad \hat{\sigma} = \sigma \frac{\tau}{\mu} \sqrt{1-a^2}. \quad (2.15d)$$

After rescaling, Eqs. (2.11) become

$$\mathcal{L}_x \hat{Z} = \frac{4\hat{D}q^2 e^{-2qx}}{1-a^2} (\hat{W} + a\hat{Z})a \quad (2.16a)$$

$$\mathcal{L}_x \hat{W} = \hat{\gamma} \hat{S} - \frac{4\hat{D}q^2 e^{-2qx}}{1-a^2} (\hat{W} + a\hat{Z}) \quad (2.16b)$$

$$\mathcal{L}_x \hat{S} = \hat{\gamma} (1 - \hat{W}) - \frac{4\hat{D}q^2 e^{-2qx}}{1-a^2} \hat{S}, \quad (2.16c)$$

with

$$\mathcal{L}_x \equiv \partial_t + 1 - \hat{D}e^{-2qx} \partial_x^2. \quad (2.17)$$

The local strain rate and torque (Eqs. 2.6, 2.10) may be written as

$$\epsilon \hat{\gamma} = \hat{\Gamma} e^{-2qx} - \hat{S} \quad (2.18)$$

$$\hat{\Gamma} = \frac{2q}{1-e^{-2q}} \left(\langle \hat{S} \rangle - \epsilon \hat{V} \right), \quad (2.19)$$

where

$$\langle \hat{S} \rangle = \int_0^1 dx \hat{S} \quad (2.20)$$

$$\hat{V} = \frac{1}{q} \int_{R_1}^{R_2} \hat{\gamma} \frac{dr}{r} = \int_0^1 dx \hat{\gamma}, \quad (2.21)$$

and

$$\epsilon = \frac{\eta}{\mu} \quad (2.22)$$

is the viscosity ratio.

We consider the dynamics of flows for prescribed histories of inner cylinder velocities \hat{V} , by solving Eqs. (2.16,2.18,2.19). The only parameters are \hat{D} , which sets the length scale of any interfaces; the slip parameter a ; the viscosity ratio ϵ ; and the curvature of the Couette cylinders, determined by q . We will often use the relative gap size,

$$p \equiv e^q - 1 \quad (2.23)$$

$$= \frac{R_2 - R_1}{R_1} \quad (2.24)$$

instead of q .

2.3. Boundary Conditions

While the fluid velocity is taken to obey no-slip boundary conditions, for Σ we choose the following boundary condition:

$$\nabla \Sigma_{\alpha\beta} = 0, \quad (2.25)$$

or

$$\partial_x \hat{W} = \partial_x \hat{Z} = \partial_x \hat{S} = 0. \quad (2.26)$$

For the interpretation of the stress diffusion term as arising from the diffusion of polymeric dumbbells (El-Kareh and Leal, 1989), this corresponds to a zero flux boundary condition. In a more realistic model gradient terms are expected to arise from inter- and intra-molecular interactions as well as center-of-mass diffusion, and the boundary condition may be a fixed non-zero gradient, or perhaps a fixed value for the stress. Clearly the boundary conditions depend on the detailed physics. In this work the nature of the boundary condition is expected to play a role in the limit when the interface touches the wall, so predictions in this limit may be non-universal.

3. COUETTE FLOW WITH NO DIFFUSION:

$$\hat{D} = 0$$

3.1. Steady State Solutions

The steady states and stability of the local JS model ($\hat{D} = 0$) in planar shear flow have been studied by many authors. Although some numerical calculations have shown well-defined shear banding (Español, Yuan and Ball, 1996; Yuan, 1999), it is generally believed that the local model supports shear bands at any stress in the non-monotonic region (Renardy, 1995; Spenley et al., 1996; Georgiou and Vlassopoulos, 1998; Lu et al., 1999). In the presence of the diffusion term stress is selected at a well defined value, independent of history. We will not discuss the case of $\hat{D} \neq 0$ in planar flow in detail here, but refer the reader to Lu et al. (1999).

Greco and Ball (1997) performed start-up calculations for $\hat{D} = 0$ in a cylindrical Couette geometry and found, unlike the 1+1D planar simulations (Spenley et al., 1996; Español et al., 1996), an apparently reproducible steady state with two shear bands and a single zero width interface between bands. Before studying this model in detail, we present a graphical construction of the steady state banded solutions.

The steady state solutions to Eqs. (2.16) for $\hat{D} = 0$ have the local form as the flat case, given by (Greco and Ball, 1997)

$$\hat{Z} = 0 \quad (3.1a)$$

$$\hat{W} = \hat{\gamma} \hat{S} \quad (3.1b)$$

$$\hat{S} = \frac{\hat{\gamma}}{1 + \hat{\gamma}^2}. \quad (3.1c)$$

Using the local force balance, Eq. (2.6), and Eq. 3.1 c) we obtain:

$$\hat{\Gamma} = \hat{r}^2 \hat{\gamma} \left(\epsilon + \frac{1}{1 + \hat{\gamma}^2} \right), \quad (3.2)$$

where

$$\hat{r} = \frac{r}{R_1}. \quad (3.3)$$

Eq. (3.2) defines the locus of steady states parametrized by torque, radial position, and local strain rate. In the

three-dimensional space spanned by $\{\hat{\Gamma}, \hat{\gamma}, r\}$ this relation defines a surface, shown in Fig. 2a. Imposing the uniform torque condition (the intersection of the surface $\hat{\Gamma}(r, \hat{\gamma})$ with a plane) yields a local relation between strain-rate and radius $\hat{\gamma}(r, t)$, shown in Fig. 2b,c.

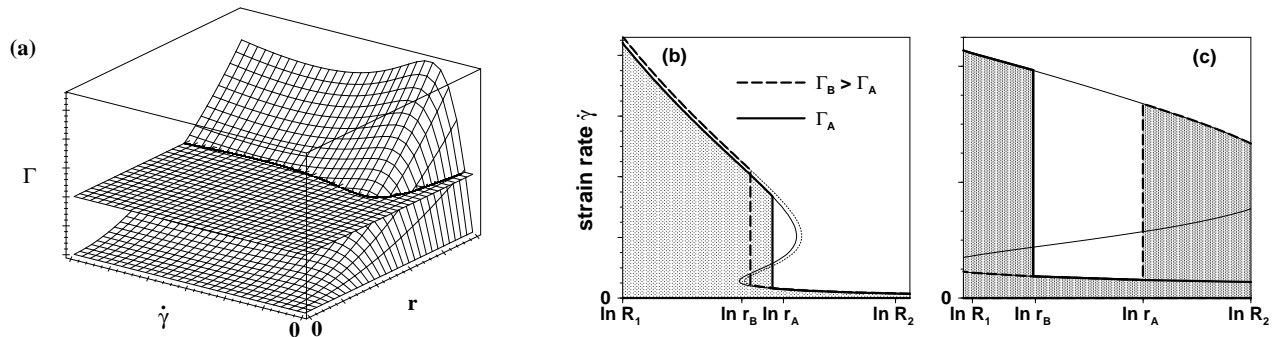


FIG. 2. (a) The curved surface shows the torque $\hat{\Gamma}(r, \hat{\gamma})$ as a function of strain-rate $\hat{\gamma}$ and radius r for the Johnson-Segalman model in Couette flow, given by Eq. (3.2). The plane is at a specified torque. (b,c) Banding profiles at different torques for the JS model in Couette flow, with no diffusion term ($\hat{D} = 0$), obtained from the intersection of the plane and curved surfaces in (a) according to Eq. (3.2). Thin lines are strain-rate $\hat{\gamma}$ as a function of radius r ; thick lines are banding solutions. (b) Possible profiles for torques Γ_A and $\Gamma_B > \Gamma_A$ at the same gap velocities V , given by the area of the shaded region. (c) Two possible bands for a given torque, again with the same gap velocity.

A steady state banded flow profile traces a trajectory $\hat{\gamma}(r)$ in Fig. 2b, with a vertical jump. In the two solutions shown in Fig. 2b, the high strain rate phase lies nearest the inner cylinder. Because of the inhomogeneity of Couette flow the high and low strain rate phases are non-uniform.

Given a solution, *e.g.* the solid line in Fig. 2b for torque $\hat{\Gamma}_A$, the shaded area corresponds to \hat{V} , according to Eq. (2.21). By placing the interface at different positions, we can generate a continuum of solutions with different gap velocities for a given torque. Conversely, it is easy to find a continuum of torques for a given gap velocity, with each torque corresponding to a unique interface position. Upon increasing the torque to $\hat{\Gamma}_B > \hat{\Gamma}_A$ while keeping the interface fixed (specified by the vertical solid line), the area under the new $\hat{\gamma}(r)$ curve, and hence the gap velocity \hat{V} , increases. To recover the \hat{V} we must move the interface closer to the inner cylinder (R_1), obtaining the solution shown in the thick dashed line. Also, multiple interface solutions are possible: flow profiles which traverse between high and low strain rate branches an odd number of times are possible steady states. Hence, for a band sequence the steady state is completely defined by any two of the three quantities Γ , V/R_1 , and interface position r_* . If both the low and high strain branches span the gap (Fig. 2c), which happens for a small curvature (R_1/R_2 close to 1), both the conventional band sequence, and an inverted band sequence, with the high strain rate material at the outer cylinder, are possible. This possibility is stabilized for flatter cylinders, and in the planar limit the conventional and inverted bands are

symmetry-related partners.

Hence, a prescribed gap velocity does not select a unique stress (torque) in cylindrical Couette geometry. At fixed V , the family of single interface steady flow solutions is parametrized by Γ or by $r_* \in [R_1, R_2]$. In principle, a universal banded steady flow might still exist if all the initial conditions or flow histories evolved to the same steady state configuration (selected values of r_* and Γ). To explore this we next simulate flows prepared by different flow histories.

3.2. Dynamics

1. History dependence

We have evolved Eqs. (2.16) through various sequences of gap velocities $\{\hat{V}(t_i)\}$, where t_i is the time when the gap velocity is changed, and considered four types of flow histories:

1. **Jump-up:** jump each time from a gap velocity \hat{V}_{down} , small and on the low strain rate branch, to a gap velocity \hat{V}_i ; $\{\hat{V}(0) = \hat{V}_{down}, \hat{V}(t_1) = \hat{V}_1, \hat{V}(t_2) = \hat{V}_{down}, \dots, \hat{V}(t_{2n}) = \hat{V}_{down}, \hat{V}(t_{2n+1}) = \hat{V}_n\}$. In particular $\hat{V}_{down} = 0$ means starting from rest.
2. **Jump-down:** jump each time from a velocity \hat{V}_{up} , large and always on the high strain rate branch, to a velocity \hat{V}_i ; $\{\hat{V}(0) = \hat{V}_{up}, \hat{V}(t_1) = \hat{V}_1, \hat{V}(t_2) = \hat{V}_{up}, \dots, \hat{V}(t_{2n}) = \hat{V}_{up}, \hat{V}(t_{2n+1}) = \hat{V}_n\}$.

3. **Ramp-up:** increasing sequence of velocity values; $\{\hat{V}(0) = 0 < \hat{V}(t_1) = \hat{V}_1 < \dots < \hat{V}(t_n) = \hat{V}_n\}$.
4. **Ramp-down:** decreasing sequence of velocity values; $\{\hat{V}(0) = \hat{V}_n > \hat{V}(t_1) = \hat{V}_{n-1} > \dots > \hat{V}(t_{n-1}) = \hat{V}_1\}$.

The lengths $t_i - t_{i-1}$ of the relaxation intervals were chosen to be much larger than the characteristic re-

laxation time for each velocity change, in order to obtain the steady state at the end of each interval. We use an implicit Crank-Nicholson algorithm to perform the dynamics. At each time step we must determine the torque $\hat{\Gamma}$ through the non-local integral condition, Eq. (2.19). For comparison, we note that Greco and Ball (1997) performed a similar calculation using $\epsilon = 0.05$ and $p = 0.1, 0.02, 0.01$, and starting from rest.

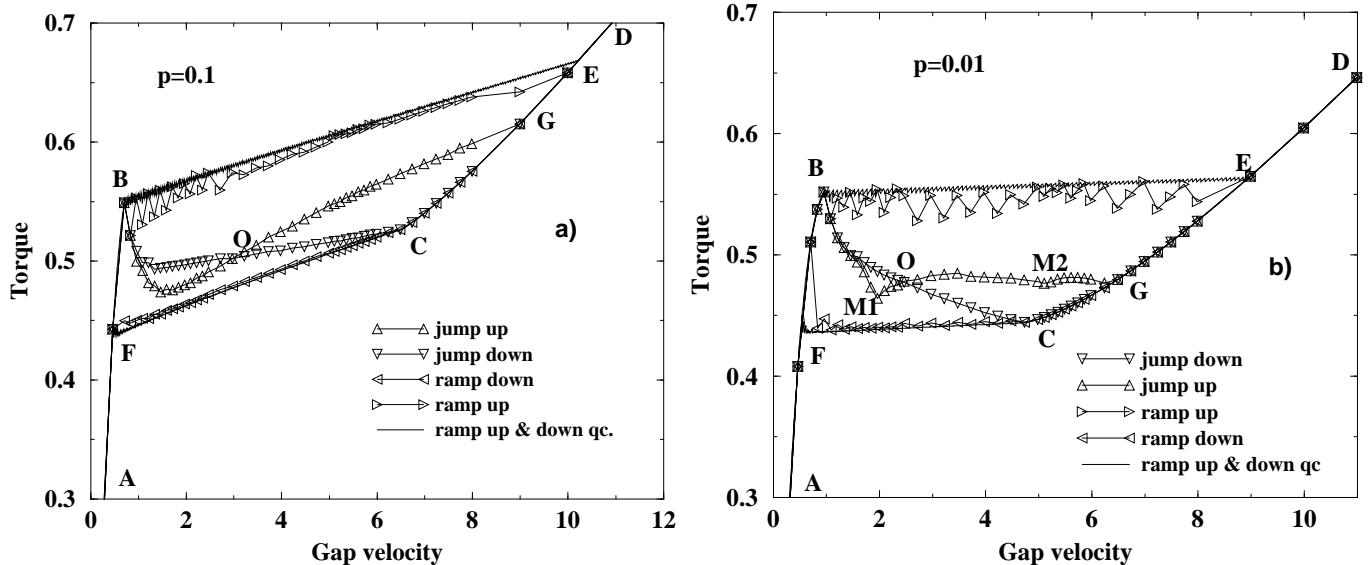


FIG. 3. Torque vs. gap velocity for the four scenarios described in the text, for $\hat{D} = 0$ and $\epsilon = 0.05$. a) $p = 0.1$; b) $p = 0.01$. $\hat{V}_{down} = 0.0$, $\hat{V}_{up} = 12.0$, the spatial mesh is 200, the time step is 0.005, and 10000 time steps assured steady state at each value for \hat{V} . Ramps are shown for both large ($d\hat{V} \gtrsim 0.2$) and quasi-continuous ($d\hat{V} \simeq 0.01$, denoted **qc**) velocity changes.

The steady state values of $\hat{\Gamma}$ at a given gap velocity \hat{V} are history dependent, as shown in Fig. 3. For the same gap velocity, steady flows obtained via different scenarios differ by the number of bands and the proportion of high shear rate band. For high curvatures steady banded flow has two bands for all scenarios, with the high shear rate band at the inner cylinder, but the amount of high shear rate band for the same gap velocity is maximum (the torque is minimum) on ramp-down, minimum on ramp-up, and takes different intermediate values for jump-up and jump-down scenarios. The case of low curvature $p = 0.01$ provides a surprise in jump-up from rest, also noted by Greco and Ball. Within the interval $1.96 < \hat{V} < 5.1$ (between points M1 and M2 in Fig. 3b) the steady state contains two interfaces, separating an interior high strain rate band from two outer low strain rate bands against the cylinder walls. For $0.95 < \hat{V} < 1.96$ (between points B and M1 in Fig. 3b) we obtain the usual high-low two-band sequence, while for $5.1 < \hat{V} < 6.48$ (between points M2 and O in Fig. 3b) the two-band sequence is inverted (low-high) with the low strain rate band of material at the inner cylinder. The three-band region is separated from the two-band region by discontinuities of the slope, $d\hat{\Gamma}/d\hat{V}$ (points M1,

M2). The values of the gap velocity separating these different types of steady flow correspond to local minima of the torque $\hat{\Gamma}(\hat{V})$ (Fig 3b). The time development of two-band and three-band profiles can be seen in Fig. 4. The other three scenarios produce the normal two band sequence high-low.

Finally, another history-dependent feature occurs on ramp-up and ramp-down scenarios. The size of the high shear rate band in steady banded flow and therefore the torque value depends on the magnitude of the differences $\hat{V}(t_{i+1}) - \hat{V}(t_i)$ between successive velocities. If the velocity is changed quasi-statically (infinitesimal changes of \hat{V}), flow curves are smooth and correspond to top and bottom jump (the total shear stress at the position of the interface corresponds to the maximum and minimum values of the local constitutive relation) on ramp-up and ramp-down respectively. Large velocity changes produce spikes in the flow curve, both on ramp-up and ramp-down. The reason for this is the pinning of the interface at a stress value which is lower than the maximum allowed value or higher than the minimum allowed value, and has been also noticed by Spenley et al. (1996) for a different diffusionless model.

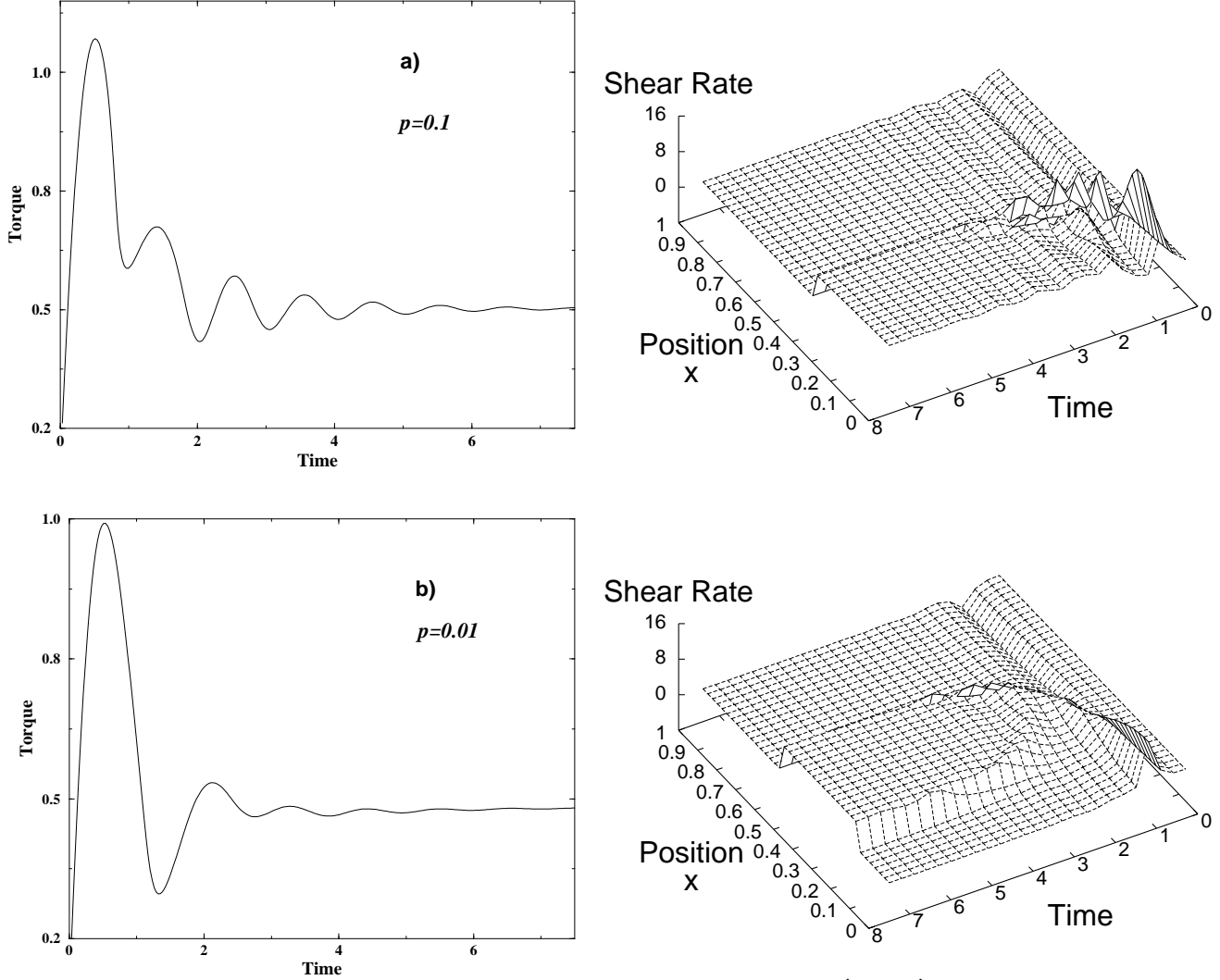


FIG. 4. Torque vs. time and strain rate vs. time jumping up from rest for $\hat{D} = 0, \hat{V} = 3.0, \epsilon = 0.05$, and a) $p = 0.1$, b) $p = 0.01$. Spatial mesh of 200 points, time step 0.00015.

2. Noise effects

The dynamical selection of steady states in the four scenarios is unstable with respect to noise in the initial conditions. To show this we used perturbed initial conditions at each new velocity value, in the form

$$\Sigma_i^{(j)}(r) = \Sigma_{i-1}^{(j)}(r; \infty) + \eta^{(j)}(r), \quad (3.4)$$

where $\Sigma_{i-1}^{(j)}(r; \infty), j = 1, 3$ are the three steady-state components of the material stress obtained at step $i-1$, and $\eta^{(j)}(r)$ are random, uniformly distributed in the interval $(-\eta_{max}, \eta_{max})$ and uncorrelated, $\langle \eta^{(j)}(r) \eta^{(j')}(r') \rangle = 0$ for $r \neq r', j \neq j'$. Fig. 5 shows the result of two-state experiments ($i = 1, 2$), starting from rest (state $i = 1$). A region in the high strain rate band close to the position of the interface (that would be selected without noise) is unstable with respect to noise,

and breaks up into many bands whose widths are limited only by the mesh size. The size of the unstable region increases with the amplitude η_{max} of the noise and it is smaller for higher curvature ($p = 0.1$). Diffusionless dynamics of the banded flow is more stable in high curvature Couette cell, as suggested by Greco and Ball (1997).

3. Basins of attraction and continuous degeneracy of steady banded flows

The dynamical equations (2.16) with $\hat{D} = 0$ correspond to an infinite dimensional nonlinear dynamical system. The dynamics in the functional space of banded flows has a complex structure of attractors (steady banded flows). Without noise, certain classes of trajectories, corresponding to initial conditions inside basins of attraction, reach

the same steady state. The jump-up branch BG (Fig. 3) is a set of attractors, collecting trajectories starting on the low shear rate branch. For an imposed gap velocity \hat{V}_{end} in the banded regime, jumping up from an initial homogeneous steady state of gap velocity $\hat{V}_{down} < \hat{V}_F$ (initial state below the point F on the flow curve, Fig. 6a) leads to an identical final banded steady state (point E_1). For higher initial gap velocities $V_F < \hat{V}_{down} < V_B$ (initial states between points F and B on the flow curve, Fig. 6a)

the final torque spans the interval $E_1 - E_2$ between the jump-up and jump-down branches (the discreteness in Fig. 6 is a finite mesh effect). The jump-up from rest branch is thus the lower limit of a continuous family of jump-up attractors. Similarly, jumping-down from a velocity $\hat{V}_{up} > V_G$ ends on the attractor branch BC which represents the upper limit of jump-down attractors which collect trajectories with $\hat{V}_{up} < V_G$ (Fig. 6).

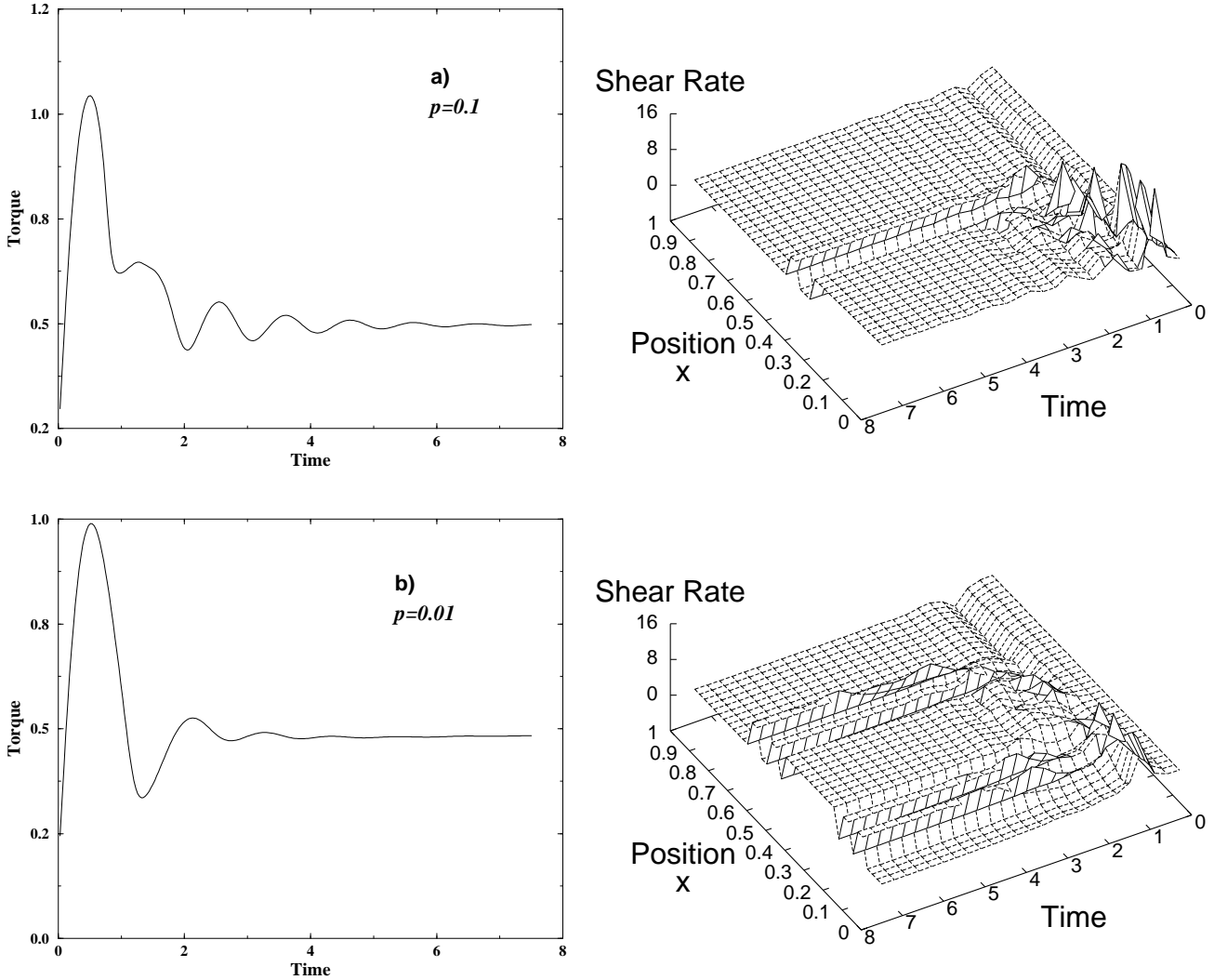


FIG. 5. Torque vs. time and strain rate vs. time for $\hat{D} = 0$, $\hat{V} = 3.0$, $\epsilon = 0.05$, and noisy initial conditions, jumping up from rest. a) $p = 0.01$, $\eta_{max} = 0.01$, time step 0.00015; b) $p = 0.1$, $\eta_{max} = 0.05$, time step 0.00015. Mesh of 200 space points.

Despite the interesting structure of these dynamics, experiments on wormlike micelles invariably display unique banding flows, independent of history and initial conditions. This is incompatible with the numerical results obtained for $\mathcal{D} = 0$; as we shall see in the following,

the imposition of non-vanishing stress diffusion $\mathcal{D} \neq 0$ provides a route for constructing unique banding flows (El-Kareh and Leal, 1989; Olmsted and Lu, 1997; Lu et al., 1999).

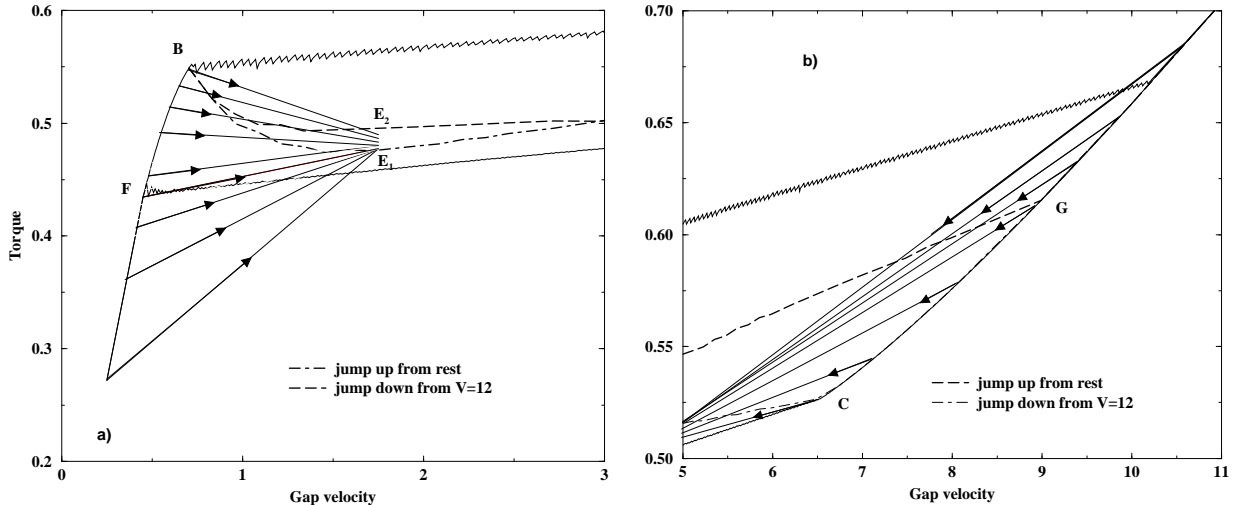


FIG. 6. Structure of basins of attraction. The arrows lines connect start and end states (attractors) upon (a) Jumping up from the low shear rate band ($\hat{V}_{end} = 1.75$) (b) Jumping down from the high shear rate band ($\hat{V}_{end} = 5$).

4. COUETTE FLOW WITH DIFFUSION: $\hat{D} \neq 0$

4.1. Flow curves and History independence

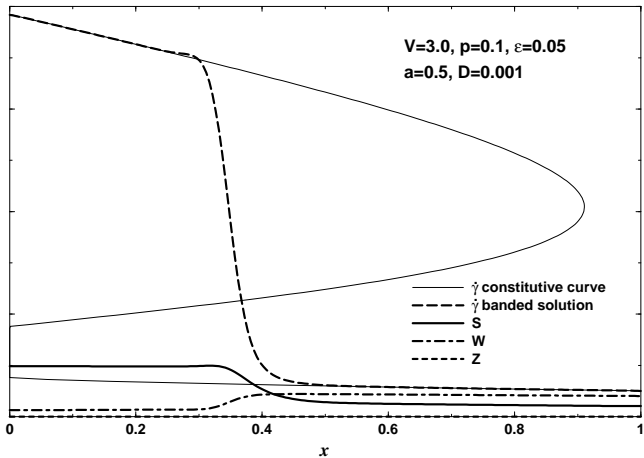


FIG. 7. Profiles for a typical steady state banded solution. Shown are the local constitutive relation and banded strain rate profile, analogous to those in Fig. 2, as well as the components \hat{S} , \hat{W} , \hat{Z} of the polymer stress, as a function of the spatial coordinate x .

We have repeated the four histories with $\hat{D} \neq 0$. In this case banded profiles are smooth, as shown in Fig. 7. The local strain rate $\hat{\gamma}(r)$ follows that of either the high or low strain rate constitutive branches except for the interface region whose width scales like $\sqrt{\hat{D}}$. The flow curves are shown in Fig. 8; as can be seen, the flow curves are essentially history-independent. Our main result is that even a small diffusion term lifts the continuous degeneracy of steady states. We shall see that this occurs by selecting the value of the total shear stress at the position of

the interface, with a selected stress σ_{sel} independent of imposed gap velocity, interface position, curvature, or \hat{D} .

In contrast to planar flow, for which the flow curve has a flat stress plateau, in cylindrical Couette flow the torque in the banding part of the flow curve has a slight dependence on the imposed gap velocity (Fig. 8). This is a consequence of the relation $\hat{\Gamma} = \hat{\sigma}_{sel} \hat{r}_*^2$, with $\hat{\sigma}_{sel}$ the selected stress at the interface position \hat{r}_* , the latter which increases from 1 to $1 + p$ as the fast-flowing band gradually fills the gap with increasing gap velocity \hat{V} . The slope of the plateau, $d\hat{\Gamma}/d\hat{V} \sim p$, vanishes in the planar limit of a thin gap. This provides a second mechanism for a sloped plateau, in addition to the effects of a concentration difference between the banding states $\hat{\Gamma}(\hat{V})$ (Schmitt, Marques and Lequeux, 1995; Olmsted and Lu, 1997).

The history independence and uniqueness of banded steady flow is shown by the coincidence of the segment $G_1 - G_2$ in Fig. 8a for all scenarios and high curvature $p = 0.1$. However, some history dependence remains for small curvatures, as seen by the two plateaus $G_1 - O - G_3$ and $G_5 - O - G_4$ for $p = 0.01$ (Fig. 8b). The positive slope plateau $G_1 - O - G_3$ corresponds to the conventional two-band flow with the high shear rate band at the inner cylinder, while for the negative slope plateau $G_5 - O - G_4$ the band sequence is inverted. The normal band sequence can be obtained by jumping up from rest for small gap velocities (between G_1 and O) and the inverted sequence can be obtained by jumping up from rest only for high gap velocities (between O and G_4). In order to scan the entire lengths $G_1 - G_3$ and $G_4 - G_5$ of the plateaus, ramping is necessary after jumping up, as shown in Fig. 8. We have checked that both band sequences are linearly stable by considering small perturbations of the interface position and shear rate. Nevertheless, as discussed in (Radulescu and Olmsted, 1999), the inverted band sequence is only metastable and nucleation processes may

change the band sequence. An inverted band is possible when both the high and low strain rate branches of the constitutive curve span the entire gap, as in Fig. 2c. There has been no experimental evidence yet for the exist-

tence of the metastable inverted band sequence, but this could be because either most experiments are performed by jumping up at low \hat{V} , or apparatus noise and interface oscillations destabilize the inverted band sequence.

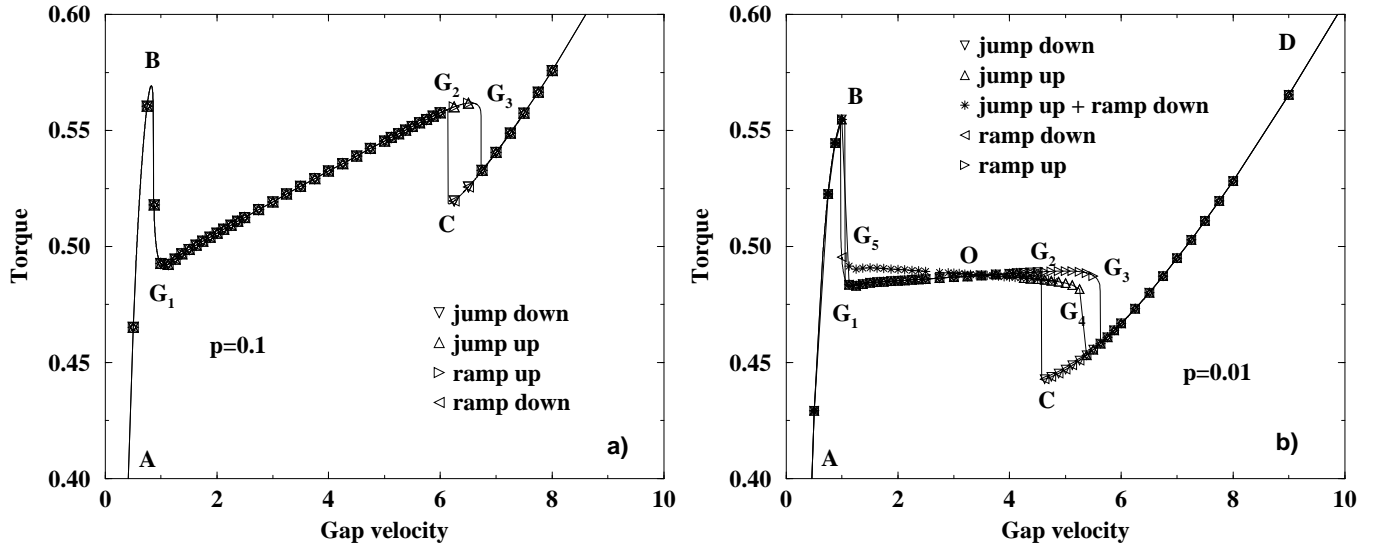


FIG. 8. Torque vs. gap velocity for a finite diffusion coefficient $\hat{D} = 0.005$, $\hat{V}_{down} = 0.0$, $\hat{V}_{up} = 12.0$. a) $p = 0.1$, 20000 time steps, b) $p = 0.01$, 40000 time steps. The spatial mesh is 400 points, with a time step of 0.005.

4.2. Selection mechanism

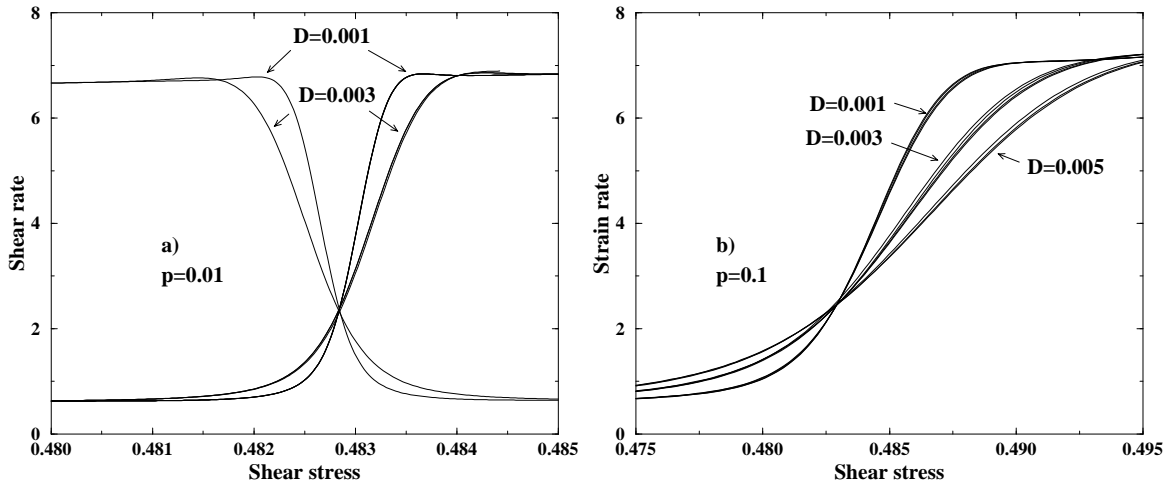


FIG. 9. Several interface profiles in the representation $\hat{\gamma}(\hat{\sigma})$. (a) two different sequences of the bands (high-low and low-high), $p = 0.01$, $\hat{V} = 1.5, 2.5, 3.5, 4.75$ and $\hat{D} = 0.001, 0.003$; (b) $p = 0.1$ and $\hat{D} = 0.001, 0.003, 0.005$ and $\hat{V} = 2.0, 3.0, 4.0, 5.0, 6.0$. For a given \hat{D} the profiles for different \hat{V} differ imperceptibly.

The key feature of stress selection by diffusion is that a stationary interface is stable only at the unique position r_* inside the gap corresponding to a selected value $\hat{\sigma}_*$ (as long as r_* is a distance from the walls which is large compared to the interface width). A rigorous proof of this property does not exist in the case of J-S model,

but justifications can be found in Lu et al. (1999), and Radulescu and Olmsted (1999). To check this we have represented the steady shear rate profiles as a function of $\hat{\sigma} = \hat{\Gamma}/\hat{r}^2$ instead of \hat{r} (Fig. 9). In this representation different banded profiles for different values of \hat{V} , and hence

\hat{r}_* , practically coincide for the same value of $\hat{\mathcal{D}}$. Profiles obtained for different values of $\hat{\mathcal{D}}$ or with different band sequences intersect at the same stress $\hat{\sigma}^* \equiv \hat{\sigma}_{sel}^*$ within 0.01%, which we define as the selected stress (see Fig. 9). This selected stress is independent of the cell curvature, the diffusion coefficient $\hat{\mathcal{D}}$, and the gap velocity \hat{V} . For example, for $\epsilon = 0.05, a = 0.5$ we find a selected stress $\hat{\sigma}_{sel}^* \simeq 0.4828$, which is almost identical to the selected stress for the planar JS model for the same viscosity ratio, $\hat{\sigma}_{planar}^* = 0.4827$ (Lu et al., 1999).

Hence, for interface widths much smaller than the radii of curvature or cylinder gap, the flow is essentially homogeneous on the scale of the interface, and the interface migrates to that position in the cylinder for which the selected stress $\hat{\sigma}_{sel}^*$ obtains. The selection of $\hat{\sigma}_{sel}^*$ provides a relation $\hat{\Gamma}/\hat{r}_*^2 = \hat{\sigma}_{sel}^* = const.$ between the torque and the interface position, thus fixing $\hat{\Gamma}$ for a given gap velocity \hat{V} and band sequence. The magnitude of $\hat{\mathcal{D}}$ has negligible effect in the thin interface limit.

Stress selection has interesting consequences for the kinetics, one of which is illustrated in Fig. 10. For flows jumping up from rest with gap velocities in the banding regime, the kinetics until an interface is well-developed

are the same as the kinetics for $\hat{\mathcal{D}} = 0$, as seen by coincidence of the solid and broken curves in Fig. 10. For $\hat{\mathcal{D}} = 0$ the kinetics ends with the *formation* of one or several interfaces, while in the presence of diffusion a second stage follows in which the interface migrates to its equilibrium position at the selected stress. For cylindrical Couette flow the stress is a monotonic function of position, so this equilibrium position is unique and steady banded flow has only one interface. If multiple interfaces form the “excess” interfaces will eventually be expelled at the walls. This is the case for low curvature (Fig. 10). The three band solution obtained when $\hat{\mathcal{D}} = 0$ (Fig. 4) becomes a transient for $\hat{\mathcal{D}} \neq 0$. For low gap velocities the interface closest to the inner cylinder is expelled and the normal sequence of bands is obtained at stationarity. Note that the expulsion time increases for decreasing $\hat{\mathcal{D}}$ (compare $\hat{\mathcal{D}} = 0.0032$ and $\hat{\mathcal{D}} = 0.005$). The inverted sequence results from an initial three-band transient at higher velocities when the interface closest to the outer cylinder is eliminated. The timescale of the interface displacement is long for small $\hat{\mathcal{D}}$, so a three-band transient could have a very long life and be mistaken for steady flow.

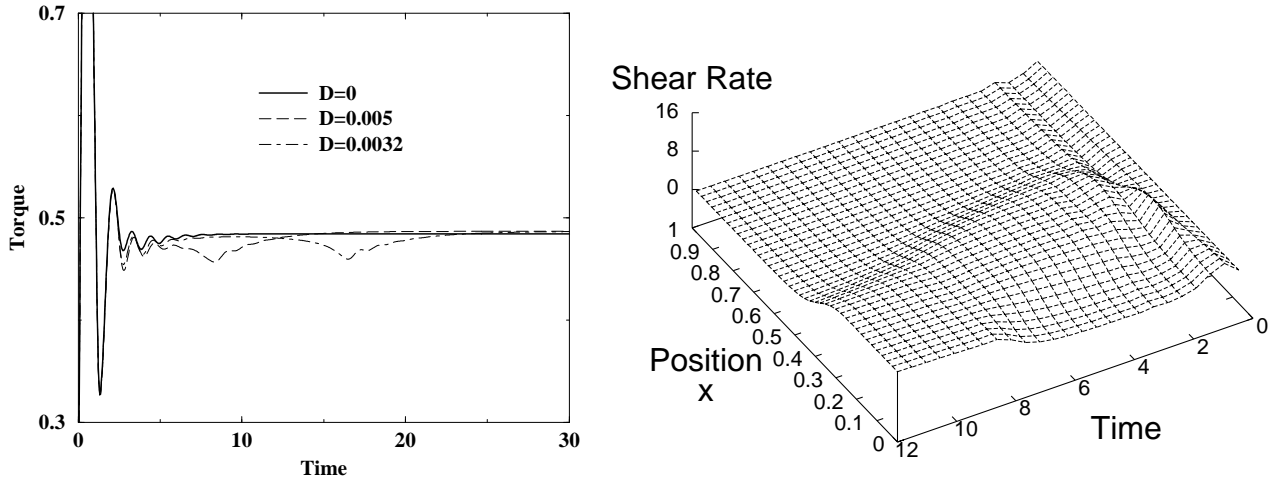


FIG. 10. (left) Strain rate vs. time for $p = 0.01, \hat{\mathcal{D}} = 0.0, 0.0032$, and 0.005 and $\hat{V} = 3.0$. (right) Torque vs. position for $\mathcal{D} = 0.005$. Elimination of the interface occurs at a local minimum (in time) of the torque. Mesh of 200 space points, time step 0.00024, for startup from rest.

4.3. Hysteresis

Ramping up and down at the extremities of the plateaus define different paths, as shown in Fig. 11: the low strain rate branch (Fig. 11a,c) or high strain rate branch (Fig. 11b,d) and the banded plateaus both possess locally stable steady state flows for a narrow range of strain rates. Upon ramping up from zero the high shear rate band begins to form at a gap velocity V_n (point B_2 in Fig. 11a) which is slightly different than the top-jump

value. V_n converges to the top-jump value when $\mathcal{D} \rightarrow 0$. On ramping back down the interface between bands is eliminated when it reaches a distance from the wall of order its width (point B_1). The difference between the corresponding gap velocity V_e and the extrapolation to the low strain rate branch scales like $\sqrt{\mathcal{D}}$. Furthermore the width of the hysteresis loops, $|V_n - V_e|$, increases with decreasing $\hat{\mathcal{D}}$, consistent with the banded plateau remaining until the interface “touches” a cylinder wall. For large enough \mathcal{D} hysteresis vanishes.

For small \mathcal{D} the hysteresis loop at the low shear rate end of the plateau contains the metastable part $B_1 - B_2$ of the low shear rate branch. This is reminiscent of the experimental results of Grand et al. (1997): under controlled strain rate conditions they found a stress (analogous to B_1 in Fig. 11a) below which the system remained

homogeneous, and above which the high strain rate band nucleated. Similar phenomena are expected at the high shear rate end of the plateau, but an experimental study of this region raises difficult problems because of various noise sources.

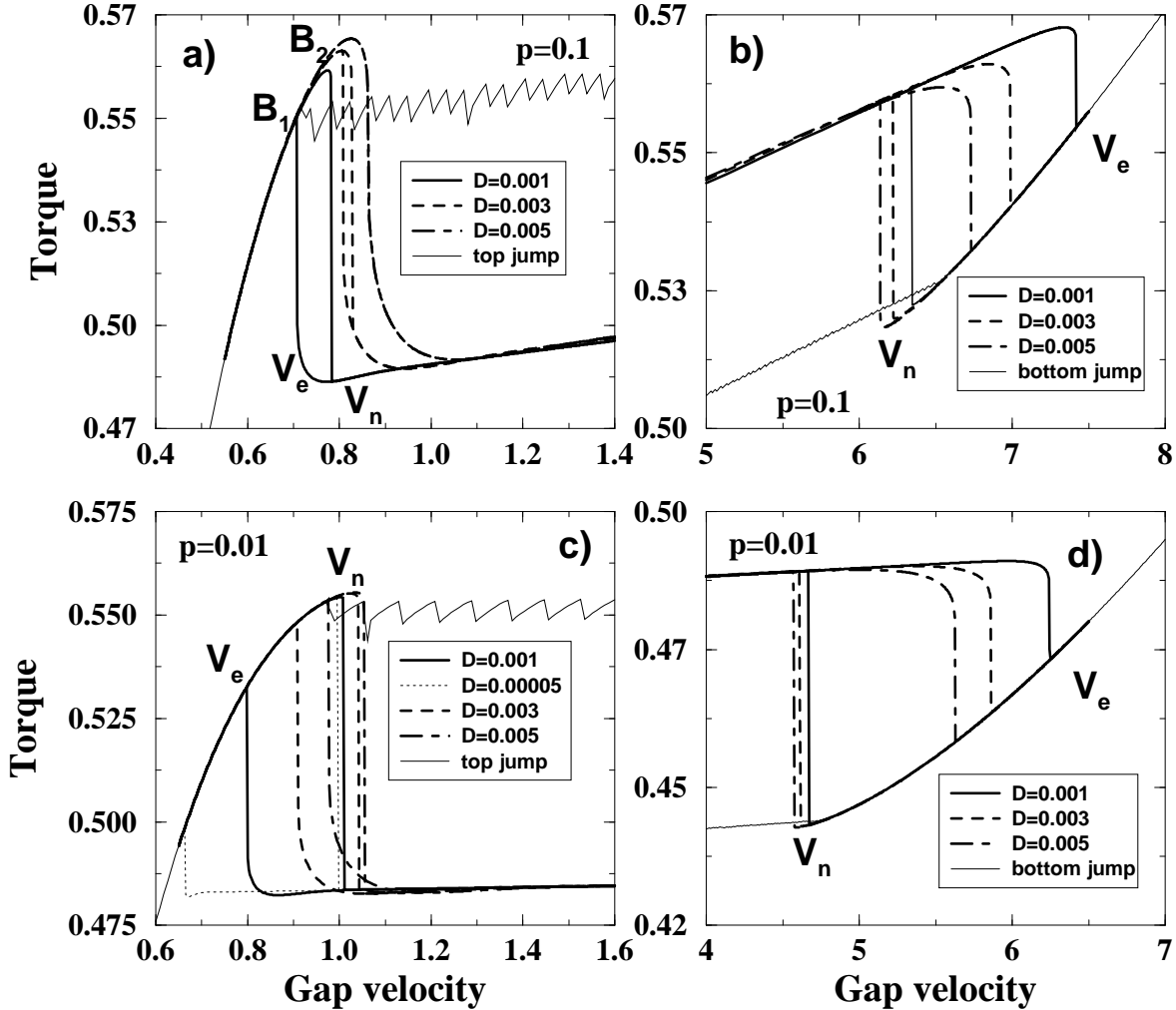


FIG. 11. Small velocity step ramping up and down ($d\hat{V} = 0.002$) in the hysteresis regions, with diffusion. a) $p = 0.1$ left end of plateau; b) $p = 0.1$ right end of plateau; c) $p = 0.01$, left end of plateau, d) $p = 0.01$, right end of plateau. The spatial mesh is 200 points, with a time step of 0.005. In all cases the diffusionless top and bottom jump are shown, respectively.

5. SUMMARY

We have studied shear banding in the local ($\mathcal{D} = 0$) Johnson-Segalman model in cylindrical Couette flow under controlled strain rate conditions. The inhomogeneous flow conditions of the Couette geometry generate history dependent steady states with a single interface of zero width. We have outlined some of the behavior under various flow histories, and identified families of attractors which govern the behavior in the absence of non-local terms in the dynamics.

To recover a unique stress and the history independence seen in experiments, it is necessary to augment local constitutive equations with non-local information. We have added a simple diffusion term and shown that the banding profile is, in the main, history independent. The steady state flow curves we have found are consistent with the growing body of work on wormlike micelles; moreover, regions of the flow curves suggest the analogs of metastability, supercooling, and nucleation and growth, and are suggestive of recent experiments on wormlike micelles (Berret et al., 1994; Berret, 1997;

Grand et al., 1997). The flow curves have a selected banding torque which increases with increasing gap velocity, with a more pronounced increase for more highly curved Couette geometries.

The diffusion term represents a singular perturbation which allows the interface to only lie at that position for which the shear stress has a well defined selected value. In the Couette geometry this position is unique, and multi-interface steady state solutions are prohibited. For flatter geometries a metastable inverted band sequence exists, with the high strain rate phase near the outer cylinder. However, there is as yet no accepted theory for diffusion terms in wormlike micelle solutions, and nor have they been measured. Our results suggest further interesting effects to study, such as band nucleation and expulsion, interface motion, and kinetics, which we hope to address in the future. For example, \mathcal{D} controls interface speed, which thus provides a possible experimental measure of this unknown quantity.

Note Added—After this manuscript was completed we learned of recent work by Yuan (1999), in which the JS model was supplemented with a diffusion term in the strain rate (effectively a non-local viscosity), and calculations were performed using a 2+1D Eulerian-Lagrangian technique in planar shear flow. Yuan also found unique stress selection in the presence of a diffusion term, but the results with no diffusive term still gave unique (and different) stress selection. This indicates that either the numerical discretization technique introduces spurious non-local terms into the dynamics, or that the larger fluctuation phase space of higher dimensions somehow stabilizes a unique stress in the absence of diffusion terms. The latter possibility appears to contradict Renardy (1995).

Acknowledgments We thank J-F Berret, G Porte, J-P Decruppe, Tom McLeish and Scott Milner for helpful discussions, and acknowledge funding from St. Catharine's College, Cambridge and the (Taiwan) National Science Council (NSC 87-2112-M-008-036) (CYDL); and EPSRC (GR/L70455) (OR, PDO).

Bagley, E. B., Cabot, I. M. and West, D. C. (1958). Discontinuity in the flow curve of polyethylene, *J. Appl. Phys.* **29**: 109–110.

Berret, J. F. (1997). Transient rheology of wormlike micelles, *Langmuir* **13**(8): 2227–2234.

Berret, J. F., Roux, D. C. and Porte, G. (1994). Isotropic-to-nematic transition in wormlike micelles under shear, *J. Phys. II (France)* **4**: 1261–1279.

Boltenhagen, P., Hu, Y. T., Matthys, E. F. and Pine, D. J. (1997). Observation of bulk phase separation and coexistence in a sheared micellar solution, *Phys. Rev. Lett.* **79**: 2359–2362.

Callaghan, P. T., Cates, M. E., Rofe, C. J. and Smeul-

ders, J. A. F. (1996). A study of the spurt effect in wormlike micelles using nuclear-magnetic-resonance microscopy, *J. Phys. II (France)* **6**: 375–393.

Cates, M. E. (1990). Nonlinear viscoelasticity of wormlike micelles (and other reversibly breakable polymers), *J. Phys. Chem.* **94**: 371.

Denn, M. M. (1990). Issues in viscoelastic fluid mechanics, *Annu. Rev. Fluid Mech.* **22**: 13–34.

Diat, O., Roux, D. and Nallet, F. (1993). Effect of shear on a lyotropic lamellar phase, *J. Phys. II (France)* **3**: 1427–1452.

Diat, O., Roux, D. and Nallet, F. (1995). Layering effect in a sheared lyotropic lamellar phase, *Phys. Rev.* **E**: 3296–3299.

Doi, M. and Edwards, S. F. (1989). *The Theory of Polymer Dynamics*, Clarendon, Oxford.

El-Kareh, A. W. and Leal, L. G. (1989). Existence of solutions for all Deborah numbers for a non-Newtonian model modified to include diffusion, *J. Non-Newton. Fl. Mech.* **33**: 257.

Español, P., Yuan, X. F. and Ball, R. C. (1996). Shear banding flow in the Johnson-Segalman fluid, *J. Non-Newton. Fl. Mech.* **65**: 93–109.

Fyrrillas, M. M., Georgiou, G. C. and Vlassopoulos, D. (1999). Time-dependent plane Poiseuille flow of a Johnson-Segalman fluid, *J. Non-Newton. Fl. Mech.* **82**: 105–123.

Georgiou, G. C. and Vlassopoulos, D. (1998). On the stability of the simple shear flow of a Johnson-Segalman fluid, *J. Non-Newton. Fl. Mech.* **75**: 77–79.

Gordon, R. J. and Schowalter, W. R. (1972). *Trans. Soc. Rheol.* **16**: 79.

Goveas, J. L. and Fredrickson, G. H. (1998). Apparent slip at a polymer-polymer interface, *Europhys. J. B* **2**: 79–92.

Grand, C., Arrault, J. and Cates, M. E. (1997). Slow transients and metastability in wormlike micelle rheology, *J. Phys. II (France)* **7**: 1071–1086.

Greco, F. and Ball, R. C. (1997). Shear-band formation in a non-Newtonian fluid model with a constitutive instability, *J. Non-Newton. Fl. Mech* **69**: 195.

Johnson, M. and Segalman, D. (1977). A model for viscoelastic fluid behavior which allows non-affine deformation, *J. Non-Newton. Fl. Mech* **2**: 255–270.

Lu, C.-Y. D., Olmsted, P. D. and Ball, R. C. (1999). The effect of non-local stress on the determination of shear banding flow, *Phys. Rev. Lett. (submitted)* **xx**: xxx–yyy.

Malkus, D. S., Nohel, J. S. and Plohr, B. J. (1990). Dynamics of shear flow of a non-Newtonian fluid, *J. Comp. Phys.* **87**: 464–487.

Malkus, D. S., Nohel, J. S. and Plohr, B. J. (1991). Analysis of new phenomena in shear flow of non-Newtonian fluids, *SIAM J. Appl. Math.* **51**: 899–929.

McLeish, T. C. B. (1987). Stability of the interface between 2 dynamic phases in capillary-flow of linear polymer melts, *J. Poly. Sci. B-Poly. Phys.* **25**: 2253–2264.

McLeish, T. C. B. and Ball, R. C. (1986). A molecular approach to the spurt effect in polymer melt flow, *J. Poly. Sci. B-Poly. Phys.* **24**: 1735–1745.

McLeish, T. C. B. and Larson, R. G. (1998). Molecular constitutive equations for a class of branched polymers: the pom-pom polymer, *J. Rheol.* **42**: 81.

Olmsted, P. D. and Goldbart, P. M. (1992). Isotropic-nematic transition in shear flow: State selection, coexistence, phase transitions, and critical behavior, *Phys. Rev.* **A46**: 4966–

- 4993.
- Olmsted, P. D. and Lu, C.-Y. D. (1997). Coexistence and phase separation in sheared complex fluids, *Phys. Rev.* **E56**: 55–58.
- Porte, G., Berret, J. F. and Harden, J. L. (1997). Inhomogeneous flows of complex fluids: Mechanical instability versus non-equilibrium phase transition, *J. Phys. II (France)* **7**: 459–472.
- Radulescu, O. and Olmsted, P. D. (1999). Matched asymptotic solutions for the steady banded flow of the diffusive Johnson-Segalman model in various geometries, *J. Non-Newton. Fl. Mech (to be published)* **xx**: xxx–yyy.
- Renardy, Y. Y. (1995). Spurt and instability in a two-layer Johnson-Segalman liquid, *The. Comp. Fl. Dyn.* **7**: 463–475.
- Roux, D., Nallet, F. and Diat, O. (1993). Rheology of lyotropic lamellar phases, *Europhys. Lett.* **24**: 53–59.
- Schmitt, V., Marques, C. M. and Lequeux, F. (1995). Shear-induced phase-separation of complex fluids – the role of flow-concentration coupling, *Phys. Rev.* **E52**: 4009–4015.
- Sierro, P. and Roux, D. (1997). Structure of a lyotropic lamellar phase under shear, *Phys. Rev. Lett.* **78**: 1496–1499.
- Spenley, N. A., Yuan, X. F. and Cates, M. E. (1996). Non-monotonic constitutive laws and the formation of shear-banded flows, *J. Phys. II (France)* **6**: 551–571.
- Vinogradov, G. V. (1972). Viscoelastic properties and flow of narrow distribution polybutadienes and polyisoprenes, *J. Poly. Sci. A* **10**: 1061.
- Yuan, X.-F. (1999). Dynamics of mechanical interface in shear-banded flow, *Europhys. Lett.* **46**: 542–548.